Location-Dependent Differences in Cardiac and Skeletal Muscle Dysfunction Associated With Truncating Titin (*ttn.2*) Variants

Celine F. Santiago[1,2] ORCID Inken G Huttner[1,2]*, Ailbhe O Brien[3]*, Pauline M. Bennett[4], Jasmina Cvetkovska[1], Renee Chand[1], Mark Holt[3] ORCID, Gunjan Trivedi[1], Louis W. Wang[1,2] ORCID, Kelly A. Smith[5] ORCID, Mathias Gautel[3] ** ORCID§ , Diane Fatkin[1,2,6] ** ORCID§ Yaniv Hinits[3] ** ORCID§

[1] Molecular Cardiology and Biophysics Division, Victor Chang Cardiac Research Institute, Darlinghurst, New South Wales, Australia.

[2] School of Clinical Medicine, Faculty of Medicine and Health, UNSW Sydney, Kensington, New South Wales, Australia

[3] Randall Centre for Cell and Molecular Biophysics, and British Heart Foundation Centre of Research Excellence, King's College London, London SE1 1UL, UK.

[4] Randall Centre for Cell and Molecular Biophysics, King's College London, London SE1 1UL, UK.

[5] Department of Anatomy & Physiology, School of Biomedical Sciences, University of Melbourne, Melbourne, Victoria, Australia.

[6] Cardiology Department, St. Vincent's Hospital, Darlinghurst, New South Wales, Australia.

Short title: *TTN*tv-associated cardiac and skeletal myopathy

* Contributed equally

** Co-senior authors

§Corresponding authors:

Mathias Gautel; e-mail: mathias.gautel@kcl.ac.uk

Diane Fatkin e-mail: d.fatkin@victorchang.edu.au

Yaniv Hinits; e-mail: yaniv.hinits@kcl.ac.uk

Randall Centre for Cell and Molecular Biophysics, New Hunt's House, 18-20 Newcomen Street, King's College London BHF Centre of Research Excellence, London SE1 1UL, UK

Abstract

Background

Truncating variants (*TTN*tv) in the *TTN* gene, encoding the giant sarcomeric protein titin, cause a range of human cardiac and skeletal muscle disorders of varying penetrance and severity. The effects of variant location on clinical manifestations are incompletely understood.

Methods

We generated six zebrafish lines carrying tv in the *ttn.2* gene at the Z-disk, I-band, A-band, and M-band titin regions. Expression of titin transcripts was evaluated using qPCR. Phenotype analysis was performed during embryonic development and in adult hearts.

Results

Using location-specific primers, we found a significant reduction of Z-disk and I-band *ttn.2* transcripts in all homozygous embryos but levels of A-band and M-band transcripts were reduced only in lines with truncations distal to the *cronos* promoter. Homozygous embryos uniformly died by 7-10 days post fertilization with marked impairment of cardiac morphology and function. Skeletal muscle motility and sarcomere organization were more disrupted in mutants with truncations distal to the *cronos* promoter compared to those proximal. The most C-terminal line (e232), which lacked only the titin kinase and M-band regions, differed from other lines, with homozygous embryos showing incorporation of truncated Ttn.2/Cronos protein and normal sarcomere assembly, but selective degradation of

fast skeletal muscle sarcomeres. Heterozygous embryos were phenotypically indistinguishable from wild-type. High-frequency echocardiography in adult heterozygous fish showed reduced ventricular contraction under resting conditions in A-band mutants. Heterozygous Z-disk and I-band mutants had no significant baseline impairment but were unable to augment ventricular contraction in response to acute adrenaline exposure, indicating a lack of cardiac reserve.

Conclusions

Our data suggest that cardiac and skeletal muscle dysfunction associated with truncating *ttn.2* variants is influenced by age, variant location, and the amount of functional titin protein. The distinctive phenotype associated with distal C-terminal truncations may reflect different requirement for C-terminal titin for maintenance of fast, slow and cardiac muscle sarcomeres.

Key words

zebrafish, titin, dilated cardiomyopathy, skeletal myopathy

73 **Introduction**

74 Titin is a giant protein that spans half-sarcomeres from the Z-disk to the M-band in the heart
75 and skeletal muscle. It is a key determinant of passive muscle stiffness and active contraction
76 in health and disease [1]. In recent years, clinical interest in titin has escalated due to
77 discoveries of genetic variants in patients with cardiac and skeletal myopathies. Truncating
78 variants in the *TTN* gene (*TTN*tv) are now known to be the most common genetic risk factor
79 for dilated cardiomyopathy (DCM) [2, 3]. While *TTN*tv-associated DCM is typically a dominant
80 adult-onset condition, albeit with variable penetrance, individuals who have two abnormal
81 *TTN* alleles leading to truncated proteins (compound heterozygotes or homozygotes) present
82 with childhood-onset skeletal myopathy [4-8]. *TTN*tv also cause cardiac and skeletal myopathy
83 in compound heterozygosity with destabilising titin missense mutations [5, 7]. *TTN*tv have been
84 reported in up to 3% of the general population [2] and frequently arise as incidental findings in
85 genetic testing for unrelated disorders and many parental carriers of *TTN*tv remain
86 asymptomatic beyond their sixties.

87 Effects due to variant location have been proposed as a useful way to stratify *TTN*tv.
88 Most DCM-associated *TTN*tv arise in the titin A-band region, while skeletal muscle-
89 associated variants were proposed to cluster in the M-band [2-4, 9]. This simplistic view does not
90 account for the presence of *TTN*tv in non-A-band locations in DCM patients, nor A-band
91 *TTN*tv in healthy subjects. Although most patients with A-band *TTN*tv have cardiac
92 presentations, there are increasing reports of overt or subclinical skeletal muscle involvement
93 [10]. Further, children with congenital recessive *TTN*tv-associated skeletal myopathy may
94 progressively develop DCM [4, 8]. There are numerous developmental and tissue-specific titin
95 isoforms that arise due to complex alternate splicing. The extent to which any single exon is
96 represented across the range of titin isoforms is indicated by the percent spliced-in (PSI)
97 score. DCM-associated *TTN*tv are thought to be preferentially distributed in exons that have

high PSI scores in adult heart [3]. Whether PSI scores are useful in the context of skeletal myopathy has yet to be clarified. Identifying the subset of *TTN*tv that have the greatest risk of pathogenicity is therefore crucial for informed medical management and genetics counselling of patients and their families.

Zebrafish are a useful animal model to study *TTN*tv effects. There are two titin genes in zebrafish, *ttn.2* (*ttna*) and *ttn.1* (*ttnb*). During early development, *ttn.2* is expressed in both cardiac and skeletal muscle and is the primary titin gene in the heart [11]. Both heart and skeletal muscle phenotypes have been reported in homozygous *ttn.2* mutants [12]. We have previously reported adult-onset DCM in heterozygous *ttn.2* zebrafish generated to carry a human A-band *TTN*tv [13]. *ttn.1* is mainly expressed in skeletal muscle and *ttn.1* mutants have been reported to have predominant skeletal myopathy phenotypes [14, 15]. An alternative promoter in *ttn.2* encodes Cronos, a short titin isoform comprising A-band and M-band domains. First discovered in zebrafish, the Cronos isoform is conserved in mouse and human [16, 17]. *Cronos* transcripts are abundant in skeletal muscle, but low in developing hearts.

The aim of our study was to investigate the impact of variant location on cardiac and skeletal muscle structure and function in embryonic and adult zebrafish, using a series of mutant lines carrying *ttn.2* variants predicted to truncate Z-disk, I-band, A-band, and M-band regions.

Methods

Detailed methods are provided in the Supplementary Material. Data are available from the corresponding authors on reasonable request.

Results

ttn.2 zebrafish models

122 We generated a series of six zebrafish *ttn.2* lines carrying variants predicted to result in a
123 truncated titin protein (Figures 1A, S1). The e5 line has a nonsense mutation that introduces a
124 premature stop codon in exon 5 before the Z-repeats in the proximal Z-disk region. The e25
125 line has a 2 bp deletion and premature stop codon in exon 25 in the proximal I-band. In the
126 e105 line, a 7 bp deletion in exon 105 is predicted to shift the reading frame with 12 residues
127 of neo-sequence followed by a premature stop codon at the amino acid corresponding to
128 human *TTNtv*, p.Y12304*. Exon 105 is in the distal I-band proximal to the *cronos* promoter.
129 The e129 line has a 5 bp deletion and stop codon in exon 129 distal to the *cronos* promoter
130 near the I-band/A-band junction. The e201 line, modelling the human *TTN*tv p.R26331*, has
131 previously been described [13] and carries an 8 bp deletion and stop codon in exon 201 in the
132 mid A-band. The e232 line has a 1 bp deletion and 8 bp insertion in exon 232 in the distal A-
133 band, upstream of the titin kinase domain and M-band [18] . Zebrafish exons targeted in these
134 mutants have high sequence homology to the corresponding human *TTN* exons, all of which
135 have high PSI scores in adult human heart (Table S5).

136 Wild-type (WT) and mutant *ttn.2* alleles were quantified by qPCR analysis of pooled
137 whole embryos (3-5 dpf). Using WT allele-specific primers, levels of WT *ttn.2* transcript
138 were reduced by ~50% in heterozygous (+/-) mutants and absent in homozygous (-/-) mutants
139 (Figure 1B). In e129-/-, e201-/- and e232 -/- embryos, titin transcripts were globally reduced
140 as indicated by qPCR using location-specific primers across Z-, I-, A- and M-band regions.
141 However, in e5-/-, e25-/- and e105-/- embryos, only Z- and I-band transcripts were reduced,
142 while A- and M-band transcripts were expressed at normal levels (Figure 1C). We
143 hypothesized that these differences might be explained by differential upregulation of the
144 titin Cronos isoform [16]. Indeed, quantification of *cronos* transcripts revealed significantly
145 increased expression in e5-/-, e25-/- and e105-/- embryos (proximal to the *cronos* promoter)
146 but not in e129-/-, e201-/- and e232-/- embryos (distal to the *cronos* promoter) (Figure 1C).

147 This may suggest up-regulation of *cronos* due to mechanism triggered by degraded mutant
148 mRNA [19]. There was modest up-regulation of the WT *ttn.1* transcript in all lines but this was
149 statistically significant only for e129-/- and e201-/- (Figure 1C).

150

151 **Embryonic cardiac phenotypes**

152 All in-crosses of heterozygous alleles gave rise to Mendelian-ratio progenies. Homozygous
153 embryos from e5, e25, e105, e129 and e201 lines were visually identified from 24 hpf by a
154 dent in the yolk caused by pericardial effusion shortly after the heart tube begins to contract
155 at 23 hpf [20]. By 3 dpf, there was severe pericardial edema, an indicator of impaired
156 ventricular contraction, as well as small eyes and craniofacial dysplasia (Figure 2A, B). The
157 heart chambers were small and linearly arranged, indicating poor development and impaired
158 looping (Figure 2B). e232-/- embryos were a notable exception, with overall wild-type
159 appearance and cardiac morphology. All homozygous embryos died between 4 to 10 dpf
160 (Figure 2C); e232-/- mutants died as larvae but survived relatively longer than other lines.
161 There were no differences in survival between heterozygotesand WT siblings.

162 Cardiac function was evaluated in embryonic fish using video-microscopy. For all
163 lines except e232, homozygous mutants showed a marked reduction in ventricular and atrial
164 contractile function (assessed by fractional area change) from 3 dpf onwards (Figure 2D, E).
165 Cardiac function in heterozygous *ttn.2* embryos was indistinguishable from WT siblings
166 (Figure S3). Heart rates were similar in WT and mutant embryos.

167

168 **Myocardial architecture in embryonic fish**

169 Embryonic hearts were evaluated using immunofluorescence staining. At 3 dpf, the intensity
170 of myosin heavy chain (MyHC) staining in e5-/-, e25-/-, e105-/-, e129-/-, and e201-/-
171 embryonic hearts was reduced, with numerous aggregates and few very disorganized fibrils

172 (Figures 3A, 3B, S4A,B). Z-disk titin interacts with the cytoskeletal protein, α-actinin [21]. In
173 e5-/-, e25-/-, e105-/-, e129-/-, and e201-/- embryos, α-actinin staining showed aggregates and
174 poorly organized striations, suggesting that some Z-I brushes may have formed in the
175 absence of titin (Figure 3A, 3B, 3D). Myosin binding protein C (MyBP-C), which is in close
176 contact with the C-zone of A-band titin [18], was absent from the cardiac sarcomeres of these
177 mutants (Figure 3C). Intriguingly, this suggests that despite the apparent absence of direct
178 titin-MyBP-C contacts in the assembled (relaxed) thick filaments, A-band titin is
179 indispensable for the correct formation of the myosin-MyBP-C complex *in vivo.* Myomesin-2
180 (Myom2) interacts with titin in the M-band in normal hearts (reviewed in [22]). Myom2 was
181 disorganized and present only at very low levels, suggestive of impaired M-band myosin-titin
182 arrays (Figure 3D).

183 Cardiac expression of Ttn.2, Ttn.1, and Cronos was evaluated using *in situ*
184 hybridization and immunostaining. In WT embryos, there was strong staining using the T12
185 antibody recognizing an epitope in I2-I3 at the start of the I-band in both Ttn.2 and Ttn.1 [23]
186 (Figure 3C), and a novel antibody that recognizes the Ttn.2 M6 M-band domain (Figures 3A,
187 S5A,B). Another antibody against the Ttn.1 M8-M9 region, but detecting both Ttn.1 and
188 Ttn.2 (Figures S2, S5A,C), showed normal cardiac staining but reduced M-band staining in
189 *ttn.1* e7-/- embryos somitic muscle sarcomeres that express both Ttn.1 and Ttn.2 (Figures
190 S2B, S6M-X). In WT embryos, *ttn.1* transcripts express only weakly in the heart at 1 dpf
191 (Figure S6B, S6D, S6F and [11]) with negligible expression by 3 dpf (Figure S6H, S6J, S6L).
192 Like previous studies [14], we found that embryonic heart development in *ttn.1* mutant lines is
193 normal (Figure S2C, C'). These finding suggest Ttn.2 but not Ttn.1 is essential for normal
194 sarcomere assembly and formation of a functional heart.

195 For all homozygous embryos except e232-/-, there was no detectable Ttn.2 protein or Ttn.1 in
196 the heart above background levels (Figure 3A, 3C and S5). Our qPCR data in whole embryos

197 (Figure 1) suggested that *cronos* upregulation might be a potential compensatory mechanism
198 for titin deficiency. However, these changes appear to be driven primarily by *cronos*
199 expression in skeletal muscle, since in situ hybridization failed to detect *cronos* in the heart
200 (Figure S6Y, S6Z and [16]).

201 In keeping with preserved cardiac function, sarcomere organization was
202 indistinguishable in T12 stained e232-/- embryos compared to WT siblings (Figure 3B).
203 Given the negligible expression of Ttn.1 and Cronos in 3 dpf hearts, we speculate that e232
204 transcripts may be incompletely degraded and that truncated e232 Ttn.2 protein is
205 incorporated into cardiac sarcomeres and able to facilitate near-normal organization of
206 myosin and sarcomeric proteins such as Myom2 (Figure 3D).

207

208 **Skeletal muscle embryonic phenotypes**

209 Skeletal muscle motility and structure was evaluated in *ttn.2* embryos. Embryos with
210 truncating variants proximal to the *cronos* promoter (e5-/-, e25-/-, e105-/-) had reduced
211 motility compared with sibling control embryos at ~24hpf, which was limited to just a tremor
212 when stimulated by touch by 3 dpf (Figure S7A). Immunofluorescence staining for myosin
213 and actin in these 3 dpf mutants showed structured sarcomeres, but some myofibrils were
214 mis-aligned and break points were evident in the middle of both slow and fast muscle fibers
215 (Figures 4A, S7B-D). MyBP-C and α-actinin appeared normal (Figure S7E, S7F).
216 Immunostaining with T12, recognizing an epitope 3' of the *ttn.2* truncation site, showed
217 strong staining in both slow and fast muscle fibers, which most likely results from Ttn.1
218 (Figures S7E and S6N, S6R, S6T, S6X). Ttn.2 M6 was also detected strongly in e5-/-, e25-/-
219 and e105-/- embryos (Figure S7F-H) and is likely to result from Cronos protein. Other M-
220 band proteins localized correctly to the M-band; Myom2 in fast muscle (Figure 4B) and
221 Myom1 in both fast and slow muscle fibers (Figure S7I-K). Overall, these data suggest that

222 Ttn.1 and Cronos have a ruler function and allow many proteins to find their position in the
223 sarcomere in the absence of full-length Ttn.2. However, reduced motility and fiber breakage
224 indicate that sarcomere structure is weaker and prone to damage once contractions
225 commence.
226
227 **Severe loss of skeletal muscle sarcomeric structure in embryos with *ttn.2* truncations**
228 **distal to the *cronos* promoter**
229 The severity of skeletal muscle phenotypes was greater in embryos with truncating variants
230 distal to the *cronos* promoter (e129-/-, 201-/-) compared to those with proximal truncations
231 (e5-/-, e25-/-, e105-/-). The former embryos were barely motile at 24 hpf, showing only weak
232 twitches. By 3 dpf, embryos were paralyzed with no response to mechano-stimulation (Figure
233 S8A). Already at 24 hpf, sarcomeres in e129-/- embryos had immature thin myofibrils
234 resembling early differentiated myofibrils [24] with only small areas of low-level sarcomeric
235 organization (Figures 4C, S8D). By 2 and 3 dpf, immunofluorescence staining for myosin
236 and actin showed a loss of axial fibrillar organization in both slow and fast fibers (Figures
237 4A, 4C, and S8B, S8C). Rather, short lengths of ~1 μm structures were revealed by staining
238 for α-actinin (Figure 4E) and antibodies that detect Ttn.1, such as Z1Z2, T12, and Ttn.1 M8-
239 M9 (Figures 4F, 4G, S8B). The directionality of these structures was random, differing
240 greatly from normal organized sarcomeres (Figure 4L, 4M) and resembling I-Z-I complexes.
241 I-Z-I complexes are structures formed during myofibrillogenesis that contain Z-disk
242 components as well as α-actin and titin. These can be put in register on actin filamentous
243 structures and can form in the absence of MyHC [25]. Ttn.2 (M6 antibody) was not detected in
244 these mutants (Figures 4E, S8E) while other M-band proteins such as Myom2 were only
245 weakly detected (Figure 4D). This suggests that fibrils expressing only Ttn.1 have lost their
246 rigidity or their ability to associate side by side, so that they grow in a wavering, random way

247 when viewed longitudinally. Electron microscopy supports this, with a few repeats of
248 sarcomere-like structures running in different directions (Figure 4H-4K). Between the Z-
249 disks and their associated thin filaments, groups of thick filaments were seen. However, they
250 did not appear to be organized as A-bands and no M-band structures were seen. Furthermore,
251 the separation of the thick filaments in cross section was greater than seen in WT siblings.
252 The sarcoplasmic reticulum was present, and some triad structures remain associated with Z-
253 disks (Figure 4J). Overall, the results show that in skeletal muscles of homozygous embryos
254 with *ttn.2* truncations distal to the *cronos* promoter, structures containing I-Z-I brushes and
255 Ttn.1 are formed, but Ttn.1 alone cannot support proper organization of A- and M-bands.
256

257 **Sarcomere structure disintegrates in fast fibers of embryos with M-band ttn.2**
258 **truncation**

259 Similar to the cardiac findings, the skeletal muscle phenotype in e232-/- embryos was distinct
260 to the other mutants. The overall appearance of e232-/- embryos was indistinguishable from
261 WT siblings at 3 dpf (Figure 2A). However, whereas coiling movement within the chorion
262 was normal at 24 hpf, e232-/- embryos had an abnormal swimming pattern at 48 hpf, which
263 involved slower tail movement and less motion of the trunk (Supplementary Video). By 5
264 dpf, e232-/- embryos lacked burst-swimming upon touch, unlike WT siblings. However,
265 spasms of the trunk, pectoral fin movement and increased eye movement in response to touch
266 were detected, indicating intact sensory reflexes (Figure S9A-S9C). Burst-swimming
267 behaviour is mediated primarily by fast fibers, whilst the early coiling movement is mediated
268 by early differentiating slow muscle [26, 27]. By 5 dpf, e232-/- mutants developed curvature of
269 the trunk and failed to inflate their swim bladders (Figure 5A, Supplementary Video) [27].

270 At 24 hpf shortly after differentiation, sarcomeric structure in both slow and fast
271 fibers in e232-/- embryos appeared normal (Figure 5B-5D). As in cardiac sarcomeres, T12

272 signal was present (Figure 5G) but Ttn.2 M6 was absent (Figure 5C), suggesting that
273 truncated Ttn.2 and Cronos were incorporated into the sarcomere. By 3 dpf, however, while
274 slow muscle fibers maintained their regular sarcomeric structure, fast muscle sarcomeres
275 were severely disrupted as indicated by myosin, MyBP-C, α-actinin and T12 (detecting Ttn.2
276 upstream from the truncation domain) staining patterns (Figures 4A, 5E-5G). The M-band
277 protein Myom1 is normally present in both slow and fast fibers but was only detected in
278 e232-/- embryo slow fibers (Figure 5E). Myom2, normally present only in fast fibers, was
279 severely diminished in e232-/- embryos (Figure 5F). Electron microscopy revealed normal
280 sarcomeric structure in e232-/- slow muscle fibers, whereas no sarcomeres were visible in
281 fast muscle fibers and thick filaments appeared to be highly disordered (Figure 5H, 5I). A
282 small number of Z-discs and triads were also visible, but not associated.
283
284 **Adult cardiac phenotypes**
285 Heterozygous *ttn.2* mutant fish survived to adulthood with overall normal appearance and
286 swimming behaviour. *ttn.2* transcript expression in mutant lines was reduced by ~50%
287 relative to WT (Figure 1B). Confirming previous studies [14], neither reduced levels of titin
288 protein nor truncated titin proteins were detectable using Western blots with an N-terminal
289 specific titin antibody, or Coomassie stained polyacrylamide gels (Figure S10). Due to the
290 lack of embryonic cardiac phenotype in e232-/- fish, e232+/- fish were not included in the
291 adult analyses.
292 Cardiac function in 12-month-old fish was evaluated using high frequency
293 echocardiography (Figure 6, Table S6). Ventricular size (EDV/BSA) in the heterozygous
294 *ttn.2* fish was unchanged compared to WT, except for e201+/- that showed modest dilatation
295 (Figure 6A), in line with our previous findings [13]. Significant impairment of ventricular
296 contractile function was seen only for e129+/- and e201+/- lines (Figure 6B through E). In

297 addition to systolic impairment, these lines also had prolonged isovolumic relaxation time,
298 indicating diastolic dysfunction (Figure 6F). Ventricular function in the A-band mutant,
299 e201+/- was similar in *ttn*^{xu071} double mutant (*ttn.2* A-band + *ttn.1* Z-disk truncations, [14]),
300 implicating predominant *ttn.2* effects (Figure S11).

301 We hypothesized that fish with *ttn.2* truncations outside the A-band might be in a
302 compensated state at baseline, and that exposure to additional stress might unmask latent
303 cardiac dysfunction. We therefore subjected 10-15 month-old e5+/- and e105+/- fish to acute
304 adrenaline stress, as previously described [28]. WT fish demonstrated the expected adrenaline-
305 induced increases in heart rate and contractility (Figure 6D-F). In contrast, these responses
306 were not seen in e5+/- and e105+/- fish (Figure 6D-F), indicating a lack of cardiac reserve.

307 Myocardial structure was further interrogated in e5+/- and e201+/- fish, hypothesizing
308 that these two lines are representative of compensated *vs.* penetrant disease states,
309 respectively. No overt differences in wall thickness or trabeculation were observed in
310 haematoxylin and eosin-stained tissue sections in either of these mutant lines relative to WT
311 siblings (Figure S12A, S12D). Sarcomere structure, content and length were also similar to
312 WT (Figure S12B-E).

313

314 **Discussion**

315 Zebrafish *TTN*tv models exhibit a varying extent of cardiac and skeletal muscle dysfunction
316 that differs with age, variant location, and the expected amount of normally functioning titin
317 protein. Previous zebrafish studies have focussed mainly on the developmental impact of titin
318 deficiency using homozygous embryos with selected Z-disk and/or A-band *ttn.2* truncations
319 [12]. We now extend these findings by directly comparing *ttn.2* truncations distributed
320 throughout the titin protein, including the first zebrafish model that truncates the M-band. We
321 also provide new data about cardiac phenotypes in a range of adult heterozygous fish. Our

322 data expand understanding of the roles of titin in heart and skeletal muscle and have potential
323 implications for human titinopathies.

324 Homozygous *ttn.2* embryos showed marked cardiac dysfunction and early death,
325 similar to reported *ttn.2* mutants [12]. These findings are most readily explained by a lack of
326 functional Ttn.2 protein in the heart and the lack of effective compensation by Ttn.1 or
327 Cronos. Homozygous *ttn.2* embryos also showed abnormalities of skeletal muscle structure
328 and function, the severity of which appeared to be determined by location with respect to the
329 *cronos* promoter. For proximal truncations, the presence of intact Cronos and Ttn.1 allows
330 formation of fragile sarcomeres that fail following onset of contraction. However, for distal
331 truncations, both Cronos and Ttn.2 are affected and although intact, Ttn.1 appears to be
332 insufficient to support viable sarcomere assembly.

333 The e232-/- embryos were a notable exception with respect to both the cardiac and
334 skeletal muscle phenotypes. A near-complete A-band in e232-/-, capable of interacting with
335 myosin and organizing MyBP-C, seems essential for incorporation and retention of truncated
336 Ttn.2 in sarcomeres. Remarkably, although loss of full-length Ttn.2 protein prevents
337 sarcomere formation, C-terminal titin appears to be dispensable for cardiomyocyte sarcomere
338 assembly, contraction, and normal heart morphology during early development. In contrast to
339 other lines, minimally truncated Ttn.2 protein is stable enough to allow integration into the
340 sarcomere. Factors such as the truncation position at the distal end of the giant titin protein
341 and the large exon size may result in reduced efficiency of nonsense mediated decay of e232
342 alleles [29]. While this might be sufficient to support sarcomere development, the presence of
343 truncated titin seems to affect protein interactions in this region. Homozygous C-terminal
344 titin truncation in mouse develop a late cardiac phenotype and differ greatly from other
345 truncations [30, 31]. Of note, sarcomeric integration of C-terminal truncated titin has been
346 reported in human muscle biopsies from patients with M-band *TTN*tv associated with

347 autosomal recessive skeletal ± cardiac myopathy [4-7].

348 In e232-/- embryos, sarcomere organization was preserved in cardiac and slow
349 muscle, but not in fast muscle fibers. Since *ttn.2* and *ttn.1* are expressed in both slow and fast
350 fibers, these observations suggest that there are fundamental differences in the requirement
351 for C-terminal titin for the assembly and maintenance in these muscle types. One difference
352 between slow and fast skeletal muscle fibers in the M-band region is expression of
353 myomesin. Whereas Myom1 is present in cardiac, slow and fast muscle in zebrafish, Myom2
354 is only expressed in fast skeletal muscle, similar to mammalian muscle (reviewed in [22]) . In
355 contrast, Myom2 is present in the murine heart from e14.5 [22], while in fish hearts, expression
356 of *myom2a*, one of the fish *MYOM2* homologues, is detected from the early embryonic heart
357 tube stage (Fig. S5AA). Collectively, our data suggest that Myom2 is not essential for
358 sarcomere assembly but may have a role in maintenance of sarcomere organization in fast
359 skeletal muscle. Other proteins that interact with M-band titin, such as obscurin, calpain-3
360 and myospryn, may be important for differentiating normally functioning sarcomeres in fast
361 versus slow and cardiac muscle fibers. Human patients with C-terminal truncations localize
362 Myom1 and obscurin/Obsl1 to the M-band, but with some disruptions [7, 32]. Similarly, e232-/-
363 mutants recruited Myom1 to slow and cardiac M-band sarcomeres, possibly via dimerization
364 of Myom1 and binding of Myom1 to obscurin/Obsl1 and myosin. However, absent M-
365 band/titin connections likely gradually result in structural instability and may underpin the
366 disruption seen in human patient samples [32]. The selective loss of fast skeletal muscle fibers
367 may reflect susceptibility to damage in response to mechanical and metabolic stress [33].
368 Interestingly, dystrophin-deficient mdx mice have disproportionate exercise-induced damage
369 in fast skeletal myofibers, and human patients with Salih myopathy and multi minicore
370 disease associated with C-terminal *TTN*tv show a predominance of slow (type I) fibers from a
371 very early age [4, 5].

372 The location of *TTN*tv has emerged as an important issue in human titinopathies.
373 Congenital skeletal titinopathy is recessive and typically associated with biallelic *TTN*tv,
374 except for a rare dominant *TTN*tv in exon 327 [34]. Cohort studies have demonstrated that these
375 disease-causing *TTN*tv can arise throughout the entire *TTN* gene [8, 35]. Cardiac involvement is
376 seen in approximately 50% patients and is more likely when both *TTN*tv are in exons that are
377 constitutively expressed in adult heart [8]. Notably, the age of disease onset is much later in
378 patients in whom at least one of the *TTN*tv is present in the last three M-band exons [35]. Two
379 autosomal dominant forms of skeletal myopathy, tibial muscular dystrophy and hereditary
380 myopathy with early respiratory failure, have been associated with single *TTN*tv in the final
381 six M-band exons [8]. These disorders typically occur in adult life and cardiac involvement is
382 variable. Taken together, these findings suggest that *TTN* location and titin "dose" are
383 important determinants of clinical manifestations and disease severity.
384 The C-terminal part of titin shows unexpected complexity in its integration into the myosin
385 filament, as revealed by recent cryo-electron tomographic (cryoET) structures. Three double
386 strands of titin (dubbed titin alpha and beta) with six molecules in total run along the thick
387 filament [18]. Both titin alpha and beta interact outside the M-band at the first levels of myosin
388 motor domains. However, whereas titin alpha continues into the M-band, the C-terminal
389 regions of titin beta from about the second Ig-domains after the kinase domain could not be
390 traced in the cryoET structure [18], suggesting that titin beta is either truncated or follows a
391 disordered path. The non-equivalence of 3 of the 6 titin filaments of each half thick filament
392 may account for the different impact of truncations N-and C-terminal to the kinase domain.
393 Structural studies of the corresponding zebrafish mutants may therefore provide valuable
394 insight into the different pathomechanism of these mutations.
395 *TTN*tv are the most common genetic cause of autosomal dominant adult-onset DCM,
396 with the majority of these being in the titin A-band or I/A junction [2, 3]. Interpretation of the

397 clinical significance of *TTN*tv outside this region has remained a clinical conundrum. Our
398 evaluation of adult zebrafish hearts confirms the importance of A-band *TTN*tv, with
399 significant changes in ventricular contraction seen under resting conditions in e129-/- and
400 e201+/- fish. However, e5+/- and e105+/- fish cannot be considered to have normal hearts as
401 their failure to augment ventricular contraction in response to an adrenaline challenge is
402 indicative of impaired contractile reserve. A recent study found that zebrafish from another
403 *ttn.2* e5+/- mutant had no overt DCM but some mild abnormalities [36]. All our zebrafish lines
404 had *ttn.2* truncating variants in zebrafish exons that show high sequence homology to
405 constitutively expressed human *TTN* exons. Collectively, our data suggest that *TTN*tv in high
406 PSI cardiac exons confer a genetic susceptibility to DCM and that overt clinical manifestation
407 may depend on patient-related factors such as age, sex, and clinical risk factors, particularly
408 those that increase cardiac mechanical stress. Further human *TTN*tv cohort studies are needed
409 to investigate these points.
410 Whereas our data, and those from human C-terminal *TTN*tvs [4-7], show clear evidence for
411 integration of truncated titin protein into the sarcomere, we have no evidence to support such
412 phenomena for more N-terminal truncations. Recent studies have reported the persistence of
413 some truncated titin protein from DCM *TTN*tv cardiomyocytes, but with conflicting evidence
414 regarding its localization in the sarcomere or in intracellular aggregates [37-40]. Our study is not
415 without limitations: there remains a lack of definitive evidence for reduced titin protein
416 expression, and for established data for titin exon usage in fetal heart and in fetal and adult
417 skeletal muscle. Due to potential species differences, our findings may not be directly
418 translatable to humans. Nevertheless, our findings provide new insights into the variability
419 underpinning *TTN*tv effects and their potential fundamental impact on thick-filament
420 assembly and are hypothesis-generating for human clinical studies.
421

Acknowledgments

We thank Dan Hesselson and Xiaolei Xu for assistance with zebrafish lines; Alexander Alexandrovich and Atsushi Fukuzawa for assistance with antigen expression and purification; Wolfgang Linke for expert assistance with titin protein analysis; the Centre for Ultrastructural Imaging, King's College London, for electron microscopy services; and the Victor Chang Cardiac Research Institute aquarium staff, in particular Aaron Hay and Cecelia Jenkin, for assistance with zebrafish husbandry. The authors acknowledge the Victor Chang Cardiac Research Institute Innovation Centre, funded by the NSW Government, including the Preclinical Imaging Facility.

Sources of Funding

AOB was supported by the PhD programme of the King's College London British Heart Foundation (BHF) Centre of Research Excellence. MG holds the BHF Chair of Molecular Cardiology. MG and YH are supported by the European Research Council Synergy Grant 856118 StuDySARCOMERE. CFS was supported by the Simon Lee Foundation and the Australian Department of Education & Training Research Training Program Scholarship. DF is supported by NSW Health, and the Medical Research Futures Fund.

Disclosures

None.

References

1. Loescher CM, Hobbach AJ, Linke WA. Titin (ttn): From molecule to modifications, mechanics, and medical significance. *Cardiovasc Res*. 2022;118:2903-2918

2. Herman DS, Lam L, Taylor MR, Wang L, Teekakirikul P, Christodoulou D, Conner L, DePalma SR, McDonough B, Sparks E, Teodorescu DL, Cirino AL, Banner NR, Pennell DJ, Graw S, Merlo M, Di Lenarda A, Sinagra G, Bos JM, Ackerman MJ, Mitchell RN, Murry CE, Lakdawala NK, Ho CY, Barton PJ, Cook SA, Mestroni L, Seidman JG, Seidman CE. Truncations of titin causing dilated cardiomyopathy. *N Engl J Med*. 2012;366:619-628

3. Roberts AM, Ware JS, Herman DS, Schafer S, Baksi J, Bick AG, Buchan RJ, Walsh R, John S, Wilkinson S, Mazzarotto F, Felkin LE, Gong S, MacArthur JA, Cunningham F, Flannick J, Gabriel SB, Altshuler DM, Macdonald PS, Heinig M, Keogh AM, Hayward CS, Banner NR, Pennell DJ, O'Regan DP, San TR, de Marvao A, Dawes TJ, Gulati A, Birks EJ, Yacoub MH, Radke M, Gotthardt M, Wilson JG, O'Donnell CJ, Prasad SK, Barton PJ, Fatkin D, Hubner N, Seidman JG, Seidman CE, Cook SA. Integrated allelic, transcriptional, and phenomic dissection of the cardiac effects of titin truncations in health and disease. *Sci Transl Med*. 2015;7:270ra276

4. Carmignac V, Salih MAM, Quijano-Roy S, Marchand S, Al Rayess MM, Mukhtar MM, Urtizberea JA, Labeit S, Guicheney P, Leturcq F, Gautel M, Fardeau M, Campbell KP, Richard I, Estournet B, Ferreiro A. C-terminal titin deletions cause a novel early-onset myopathy with fatal cardiomyopathy. *Ann. Neurol.* 2007;61:340-351

5. Chauveau C, Bonnemann CG, Julien C, Kho AL, Marks H, Talim B, Maury P, Arne-Bes MC, Uro-Coste E, Alexandrovich A, Vihola A, Schafer S, Kaufmann B, Medne L, Hubner N, Foley AR, Santi M, Udd B, Topaloglu H, Moore SA, Gotthardt M, Samuels ME, Gautel M, Ferreiro A. Recessive ttn truncating mutations define novel forms of core myopathy with heart disease. *Hum Mol Genet*. 2014;23:980-991

6. Ceyhan-Birsoy O, Agrawal PB, Hidalgo C, Schmitz-Abe K, DeChene ET, Swanson LC, Soemedi R, Vasli N, Iannaccone ST, Shieh PB, Shur N, Dennison JM, Lawlor MW, Laporte J, Markianos K, Fairbrother WG, Granzier H, Beggs AH. Recessive truncating titin gene, ttn, mutations presenting as centronuclear myopathy. *Neurology*. 2013;81:1205-1214

7. Rees M, Nikoopour R, Fukuzawa A, Kho AL, Fernandez-Garcia MA, Wraige E, Bodi I, Deshpande C, Ozdemir O, Daimaguler HS, Pfuhl M, Holt M, Brandmeier B, Grover S, Fluss J, Longman C, Farrugia ME, Matthews E, Hanna M, Muntoni F, Sarkozy A, Phadke R, Quinlivan R, Oates EC, Schroder R, Thiel C, Reimann J, Voermans N, Erasmus C, Kamsteeg EJ, Konersman C, Grosmann C, McKee S, Tirupathi S, Moore SA, Wilichowski E, Hobbiebrunken E, Dekomien G, Richard I, Van den Bergh P, Dominguez-Gonzalez C, Cirak S, Ferreiro A, Jungbluth H, Gautel M. Making sense of missense variants in ttn-related congenital myopathies. *Acta Neuropathol*. 2021;141:431-453

8. Oates EC, Jones KJ, Donkervoort S, Charlton A, Brammah S, Smith JE, 3rd, Ware JS, Yau KS, Swanson LC, Whiffin N, Peduto AJ, Bournazos A, Waddell LB, Farrar MA, Sampaio HA, Teoh HL, Lamont PJ, Mowat D, Fitzsimons RB, Corbett AJ, Ryan MM, O'Grady GL, Sandaradura SA, Ghaoui R, Joshi H, Marshall JL, Nolan MA, Kaur S, Punetha J, Topf A, Harris E, Bakshi M, Genetti CA, Marttila M, Werlauff U, Streichenberger N, Pestronk A, Mazanti I, Pinner JR, Vuillerot C, Grosmann C, Camacho A, Mohassel P, Leach ME, Foley AR, Bharucha-Goebel D, Collins J, Connolly AM, Gilbreath HR, Iannaccone ST, Castro D, Cummings BB, Webster RI, Lazaro L, Vissing J, Coppens S, Deconinck N, Luk HM, Thomas NH, Foulds NC, Illingworth MA, Ellard S, McLean CA, Phadke R, Ravenscroft G, Witting N, Hackman P, Richard I, Cooper ST, Kamsteeg EJ, Hoffman EP, Bushby K, Straub V, Udd B, Ferreiro A, North KN, Clarke NF, Lek M, Beggs AH, Bonnemann CG, MacArthur DG, Granzier H, Davis MR, Laing NG. Congenital titinopathy: Comprehensive characterization and pathogenic insights. *Ann Neurol*. 2018;83:1105-1124

494 9. Savarese M, Sarparanta J, Vihola A, Udd B, Hackman P. Increasing role of titin mutations in
495 neuromuscular disorders. *J Neuromuscul Dis*. 2016;3:293-308

496 10. Skriver SV, Krett B, Poulsen NS, Krag T, Walas HR, Christensen AH, Bundgaard H, Vissing
497 J, Vissing CR. Skeletal muscle involvement in patients with truncations of titin and familial
498 dilated cardiomyopathy. *JACC Heart Fail*. 2024;12:740-753

499 11. Seeley M, Huang W, Chen Z, Wolff WO, Lin X, Xu X. Depletion of zebrafish titin reduces
500 cardiac contractility by disrupting the assembly of z-discs and a-bands. *Circ Res*.
501 2007;100:238-245

502 12. Santiago CF, Huttner IG, Fatkin D. Mechanisms of ttntv-related dilated cardiomyopathy:
503 Insights from zebrafish models. *J Cardiovasc Dev Dis*. 2021;8

504 13. Huttner IG, Wang LW, Santiago CF, Horvat C, Johnson R, Cheng D, Frieling-Salewsky Mv,
505 Hillcoat K, Bemand TJ, Trivedi G, Braet F, Hesselson D, Alford K, Hayward CS, Seidman JG,
506 Seidman CE, Feneley MP, Linke WA, Fatkin D. A-band titin truncation in zebrafish causes
507 dilated cardiomyopathy and hemodynamic stress intolerance. *Circulation: Genomic and*
508 *Precision Medicine*. 2018;11:e002135

509 14. Shih YH, Dvornikov AV, Zhu P, Ma X, Kim M, Ding Y, Xu X. Exon- and contraction-
510 dependent functions of titin in sarcomere assembly. *Development*. 2016;143:4713-4722

511 15. Steffen LS, Guyon JR, Vogel ED, Howell MH, Zhou Y, Weber GJ, Zon LI, Kunkel LM. The
512 zebrafish runzel muscular dystrophy is linked to the titin gene. *Developmental Biology*.
513 2007;309:180-192

514 16. Zou J, Tran D, Baalbaki M, Tang LF, Poon A, Pelonero A, Titus EW, Yuan C, Shi C, Patchava
515 S, Halper E, Garg J, Movsesyan I, Yin C, Wu R, Wilsbacher LD, Liu J, Hager RL, Coughlin
516 SR, Jinek M, Pullinger CR, Kane JP, Hart DO, Kwok P-Y, Deo RC. An internal promoter
517 underlies the difference in disease severity between n- and c-terminal truncation mutations of
518 titin in zebrafish. *eLife*. 2015;4:e09406

519 17. Zaunbrecher RJ, Abel AN, Beussman K, Leonard A, von Frieling-Salewsky M, Fields PA,
520 Pabon L, Reinecke H, Yang X, Macadangdang J, Kim DH, Linke WA, Sniadecki NJ, Regnier
521 M, Murry CE. Cronos titin is expressed in human cardiomyocytes and necessary for normal
522 sarcomere function. *Circulation*. 2019;140:1647-1660

523 18. Tamborrini D, Wang Z, Wagner T, Tacke S, Stabrin M, Grange M, Kho AL, Rees M, Bennett
524 P, Gautel M, Raunser S. Structure of the native myosin filament in the relaxed cardiac
525 sarcomere. *Nature*. 2023

526 19. El-Brolosy MA, Kontarakis Z, Rossi A, Kuenne C, Gunther S, Fukuda N, Kikhi K, Boezio
527 GLM, Takacs CM, Lai SL, Fukuda R, Gerri C, Giraldez AJ, Stainier DYR. Genetic
528 compensation triggered by mutant mrna degradation. *Nature*. 2019;568:193-197

529 20. Bakkers J. Zebrafish as a model to study cardiac development and human cardiac disease.
530 *Cardiovasc Res*. 2011;91:279-288

531 21. Gautel M, Djinovic-Carugo K. The sarcomeric cytoskeleton: From molecules to motion. *J Exp*
532 *Biol*. 2016;219:135-145

533 22. Lange S, Pinotsis N, Agarkova I, Ehler E. The m-band: The underestimated part of the
534 sarcomere. *Biochim Biophys Acta Mol Cell Res*. 2020;1867:118440

535 23. Sebestyen MG, Wolff JA, Greaser ML. Characterization of a 5.4 kb cdna fragment from the z-
536 line region of rabbit cardiac titin reveals phosphorylation sites for proline-directed kinases. *J*
537 *Cell Sci*. 1995;108 (Pt 9):3029-3037

538 24. Hinits Y, Hughes SM. Mef2s are required for thick filament formation in nascent muscle fibres.
539 *Development*. 2007;134:2511-2519

25. Schultheiss T, Lin ZX, Lu MH, Murray J, Fischman DA, Weber K, Masaki T, Imamura M, Holtzer H. Differential distribution of subsets of myofibrillar proteins in cardiac nonstriated and striated myofibrils. *J Cell Biol*. 1990;110:1159-1172

26. Saint-Amant L, Drapeau P. Time course of the development of motor behaviors in the zebrafish embryo. *J Neurobiol*. 1998;37:622-632

27. Naganawa Y, Hirata H. Developmental transition of touch response from slow muscle-mediated coilings to fast muscle-mediated burst swimming in zebrafish. *Dev Biol*. 2011;355:194-204

28. Wang LW, Huttner IG, Santiago CF, Fatkin D. Bradycardia in zebrafish heart failure: A true physiological response or anesthetic-induced red herring? *Zebrafish*. 2016;13:475-476

29. Lindeboom RGH, Vermeulen M, Lehner B, Supek F. The impact of nonsense-mediated mrna decay on genetic disease, gene editing and cancer immunotherapy. *Nat Genet*. 2019;51:1645-1651

30. Radke MH, Polack C, Methawasin M, Fink C, Granzier HL, Gotthardt M. Deleting full length titin versus the titin m-band region leads to differential mechanosignaling and cardiac phenotypes. *Circulation*. 2019;139:1813-1827

31. Weinert S, Bergmann N, Luo X, Erdmann B, Gotthardt M. M line-deficient titin causes cardiac lethality through impaired maturation of the sarcomere. *J Cell Biol*. 2006;173:559-570

32. Fukuzawa A, Lange S, Holt M, Vihola A, Carmignac V, Ferreiro A, Udd B, Gautel M. Interactions with titin and myomesin target obscurin and obscurin-like 1 to the m-band – implications for hereditary myopathies. *Journal of Cell Science*. 2008;121:1841-1851

33. Lloyd EM, Pinniger GJ, Murphy RM, Grounds MD. Slow or fast: Implications of myofibre type and associated differences for manifestation of neuromuscular disorders. *Acta Physiol (Oxf)*. 2023;238:e14012

34. Claeys KG, Savarese M, Jonson PH, Goosens V, Topf A, Vihola A, Straub V, Udd B. A titin truncating variant causing a dominant myopathy with cardiac involvement in a large family: The exception that proves the rule. *Neurol Genet*. 2024;10:e200185

35. Savarese M, Vihola A, Oates EC, Barresi R, Fiorillo C, Tasca G, Jokela M, Sarkozy A, Luo S, Diaz-Manera J, Ehrstedt C, Rojas-Garcia R, Saenz A, Muelas N, Lonardo F, Fodstad H, Qureshi T, Johari M, Valipakka S, Luque H, Petiot P, de Munain AL, Pane M, Mercuri E, Torella A, Nigro V, Astrea G, Santorelli FM, Bruno C, Kuntzer T, Illa I, Vilchez JJ, Julien C, Ferreiro A, Malandrini A, Zhao CB, Casar-Borota O, Davis M, Muntoni F, Hackman P, Udd B. Genotype-phenotype correlations in recessive titinopathies. *Genet Med*. 2020;22:2029-2040

36. Zhu P, Li J, Yan F, Islam S, Lin X, Xu X. Allelic heterogeneity of ttntv dilated cardiomyopathy can be modeled in adult zebrafish. *JCI Insight*. 2024;9

37. Fomin A, Gartner A, Cyganek L, Tiburcy M, Tuleta I, Wellers L, Folsche L, Hobbach AJ, von Frieling-Salewsky M, Unger A, Hucke A, Koser F, Kassner A, Sielemann K, Streckfuss-Bomeke K, Hasenfuss G, Goedel A, Laugwitz KL, Moretti A, Gummert JF, Dos Remedios CG, Reinecke H, Knoll R, van Heesch S, Hubner N, Zimmermann WH, Milting H, Linke WA. Truncated titin proteins and titin haploinsufficiency are targets for functional recovery in human cardiomyopathy due to ttn mutations. *Sci Transl Med*. 2021;13:eabd3079

38. McAfee Q, Caporizzo MA, Uchida K, Bedi KC, Jr., Margulies KB, Arany Z, Prosser BL. Truncated titin protein in dilated cardiomyopathy incorporates into the sarcomere and transmits force. *J Clin Invest*. 2024;134

39. McAfee Q, Chen CY, Yang Y, Caporizzo MA, Morley M, Babu A, Jeong S, Brandimarto J, Bedi KC, Jr., Flam E, Cesare J, Cappola TP, Margulies K, Prosser B, Arany Z. Truncated titin proteins in dilated cardiomyopathy. *Sci Transl Med*. 2021;13:eabd7287

40. Kellermayer D, Tordai H, Kiss B, Torok G, Peter DM, Sayour AA, Polos M, Hartyanszky I, Szilveszter B, Labeit S, Gango A, Bedics G, Bodor C, Radovits T, Merkely B, Kellermayer MS. Truncated titin is structurally integrated into the human dilated cardiomyopathic sarcomere. *J Clin Invest*. 2024;134

597 **Figure legends**

598

599 **Figure 1. Zebrafish *ttn.2* truncating variants**. **A,** Schematic of the Ttn.2 protein showing
600 major domains and the *cronos* translation start site (TSS). Locations of *ttn.2* truncations (red
601 arrows) and the *ttn*^{x071} mutant [14] (asterisk) are indicated. **B,** qPCR analysis of homozygous (-
602 /-), heterozygous (+/-) and wild-type (WT; +/+) whole embryos (left panel) and adult hearts
603 (right panel) using primers specific for the wild-type allele. **C,** qPCR analysis of homozygous
604 *ttn.2* whole embryos and WT controls using primer pairs specific for various *ttn.2* and *ttn.1*
605 regions. qPCR data (**B,C**) were normalized to house-keeping genes and expressed as absolute
606 levels of abundance. Two-way ANOVA, mean ± SD.

607

608 **Figure 2. Cardiac morphology and function in homozygous *ttn.2* embryos. A,** Brightfield
609 images of 3 dpf homozygous and sibling control embryos shown in lateral view, anterior to
610 left, with (**B**) higher magnification of the heart. With the exception of e232-/-, mutant
611 embryos show pericardial edema (magenta arrowhead), as well as small eyes and head (cyan
612 arrowhead). **C,** Survival in homozygous and wild-type (WT) embryos between 0 and 20 dpf;
613 Mantel-Cox test. Ventricular (**D**) and atrial (**E**) contractile function were assessed using
614 video-microscopy. Data are expressed as fractional area change (FAC; %). Unpaired t-tests,
615 mean ± SD. A denotes atrium, OED, edema, OFT, outflow tract, and V, ventricle.

616

617 **Figure 3. Cardiac sarcomere assembly in *ttn.2* embryos. A** and **B,** Single confocal scans
618 through ventricular sarcomeres of 3 dpf homozygous and sibling (sib) control embryos,
619 immunostained for myosin heavy chain (MyHC), α-actinin, and Ttn.2 M6. Mutants show
620 punctate aggregates (arrowheads) except e232-/- embryos in which sarcomeres appear
621 normal. No titin protein is detected by Ttn.2 M6 antibodies in e129-/- hearts. **C,** Confocal

622 stacks of 3 dpf hearts of homozygous *ttn.2* and sibling control embryos, immunostained for
623 Ttn T12 and myosin binding protein-C (MyBP-C), shown in ventral view, anterior to left.
624 Heart chambers show very low levels of Ttn T12 and MyBP-C. **D**, Single confocal scans
625 through ventricular sarcomeres of e25-/-, e232-/-, and sibling control embryos,
626 immunostained for α-actinin and myomesin-2 (Myom2). e25-/- embryos show punctate
627 aggregates of α-actinin and only low levels of Myom2. In (**C**) and (**D**), cardiac morphology
628 and sarcomeres in e232-/- embryos are similar to control. A denotes atrium, SH,
629 sternohyoideus muscle, and V, ventricle.
630
631 **Figure 4. Skeletal muscle phenotypes in *ttn.2* embryos. A** through **G,** Immunofluorescence
632 staining of 3 dpf homozygous and sibling (sib) control embryos for myosin heavy chain
633 (MyHC), fast myosin light chain (Fast MyLC), α-actinin, myomesin-2 (Myom2), Ttn.2 M6,
634 Ttn T12, and Ttn.1 M8-M9, shown in lateral view, anterior to left. MyHC is strongly
635 expressed in superficial slow fibers, while MyLC labels fast fibers. **A**, e25-/- embryos show
636 some good sarcomeric structure as well as regions of damaged sarcomeres in the middle of
637 the fiber (white arrowheads). e129-/- embryos have disorganized sarcomeres in both slow
638 (yellow arrowheads) and fast fibers, while e232-/- embryos have striated slow fibers but no
639 organized thick filaments in fast fibers. **B**, In e25-/- embryos, α-actinin (slow and fast fibers)
640 and Myom2 (fast only) seem striated. **C** through **G**, In e129-/- embryos, abnormal striation is
641 detected from 24 hpf to 3 dpf; MyHC and α-actinin and show no normal striation but some
642 radial organization is seen around random points in the fiber (**C,E**), Myom2 is abolished (**D**),
643 and Ttn.2 M6 is completely missing (**E**). This abnormal striation is also seen with Ttn T12
644 (**F**) and Ttn.1 M8-M9 (**G**). **H** through **M,** Electron micrographs of longitudinal sections of 3
645 dpf e129-/- and sibling control embryos. Thin filaments in mutant embryos are arranged in I-
646 Z-I brushes that are organized in radiating patterns (**H**, red arrows), highlighting structural

647 features (**I**), including triads (blue arrowheads), Z-disks (pink arrowheads) and thin filaments
648 (cyan arrowheads). **J**, Schematic illustrating arrangement of thick and thin filaments. **K,**
649 Electron micrographs of transverse sections of fibers in 3 dpf embryos showing lattice pattern
650 of thick and thin filaments in sibling controls and increased interfilament space in e129-/-. **L**
651 and **M,** Quantification of directionality of fibres. Rose diagram of representative somitic
652 muscle (**L**) and graph comparing the variance of the orientations (**M**). The possible range is 0
653 to 1, where 0 is completely ordered and 1 is completely random. Unpaired t-tests, mean ±
654 SEM.
655
656 **Figure 5. Skeletal muscle phenotypes in e232-/- embryos. A,** Brightfield images of 5 dpf
657 e232-/- and sibling (sib) control embryos, lateral view, anterior to left. Mutants show a
658 distinctive trunk curvature (red arrowhead) and fail to inflate swim bladder (black
659 arrowheads). **B** through **G,** Immunofluorescence staining of e232-/- and sibling (sib) control
660 embryos for myosin heavy chain (MyHC), fast myosin light chain (Fast MyLC), α-actinin,
661 Ttn.2 M6, Ttn.1 M8-M9, myomesin-1 (Myom1), myosin binding protein-C (MyBP-C),
662 myomesin-2 (Myom2) and Ttn T12, shown in lateral view, anterior to left. At 24 hpf (**B-D**),
663 MyHC, fast MyLC, α-actinin and Ttn.1 M8-M9 (slow) show regular sarcomeres although
664 Ttn.2 M6 is not detected. By 3 dpf (**E-H**), Myom1 (strong in fast fibers) and MyBP-C
665 (strong in slow fibers) are present in both slow (**E**, arrows) and fast fibers (**E**, arrowheads) in
666 controls but are detected only in slow fibers in e232-/- embryos. Myom2 is expressed only in
667 fast fibers (**F**, arrowheads), whereas α-actinin is in both slow (**F**, arrows) and fast (**F**,
668 arrowheads) fibers. In e232-/- embryos, α-actinin is normal in slow fibers (arrows) but is
669 disorganized and aggregated in the deeper fast fibers. Myom2 shows diminished signal above
670 background. **G**, Fibers are scanned at different levels to highlight superficial slow muscle
671 (left panels) and deeper medial fast fibers (right panels). Ttn T12 striation patterns are similar

672 in e232-/- and control embryos in slow fibers but mutants have a punctate disorganised
673 staining fast fibers. **H** through **I,** Electron micrographs of longitudinal muscle sections of 3
674 dpf e232-/- and sibling control embryos. Control embryos have organized sarcomeric
675 structure with clear Z-disk (Z) and M-band (M) visible in both slow and fast muscle fibers.
676 e232-/- embryos have organized sarcomeres only in slow muscle fibers. Thick filaments (red
677 arrowheads) are present in mutant fast fibers but are not arranged into sarcomeres.
678 Sarcoplasmic reticulum (orange arrowheads) is disordered in mutant fast fibers. Blue kites
679 indicate EM artefacts. Triads (green arrowheads) are located at the Z-disk in control fast
680 fibers. In mutant fast fibers, there are a small number of triads and Z-disk but these are not
681 associated together.
682
683 **Figure 6. Ventricular size and function in adult heterozygous *ttn.2* zebrafish.** Cardiac
684 function was assessed in 12 month-old wild-type (WT) and heterozygous *ttn.2* fish using high
685 frequency echocardiography. **A** through **F s**how ventricular function under resting conditions:
686 **A**, indexed ventricular end-diastolic volume (EDV/BSA), **B**, ejection fraction (EF); **C**, global
687 longitudinal strain (GLS), **D**, peak ventricular outflow tract velocity (VOT), **E**, peak systolic
688 global longitudinal strain rate (GLSRs), **F**, isovolumic relaxation time (IVRT). **G** through **I**
689 show responses (at 2 hr) to acute adrenaline administration in 10-15 month-old fish. Two-
690 way ANOVA, mean ± SD, or Δmean ± SD.
691
692

Figure 1

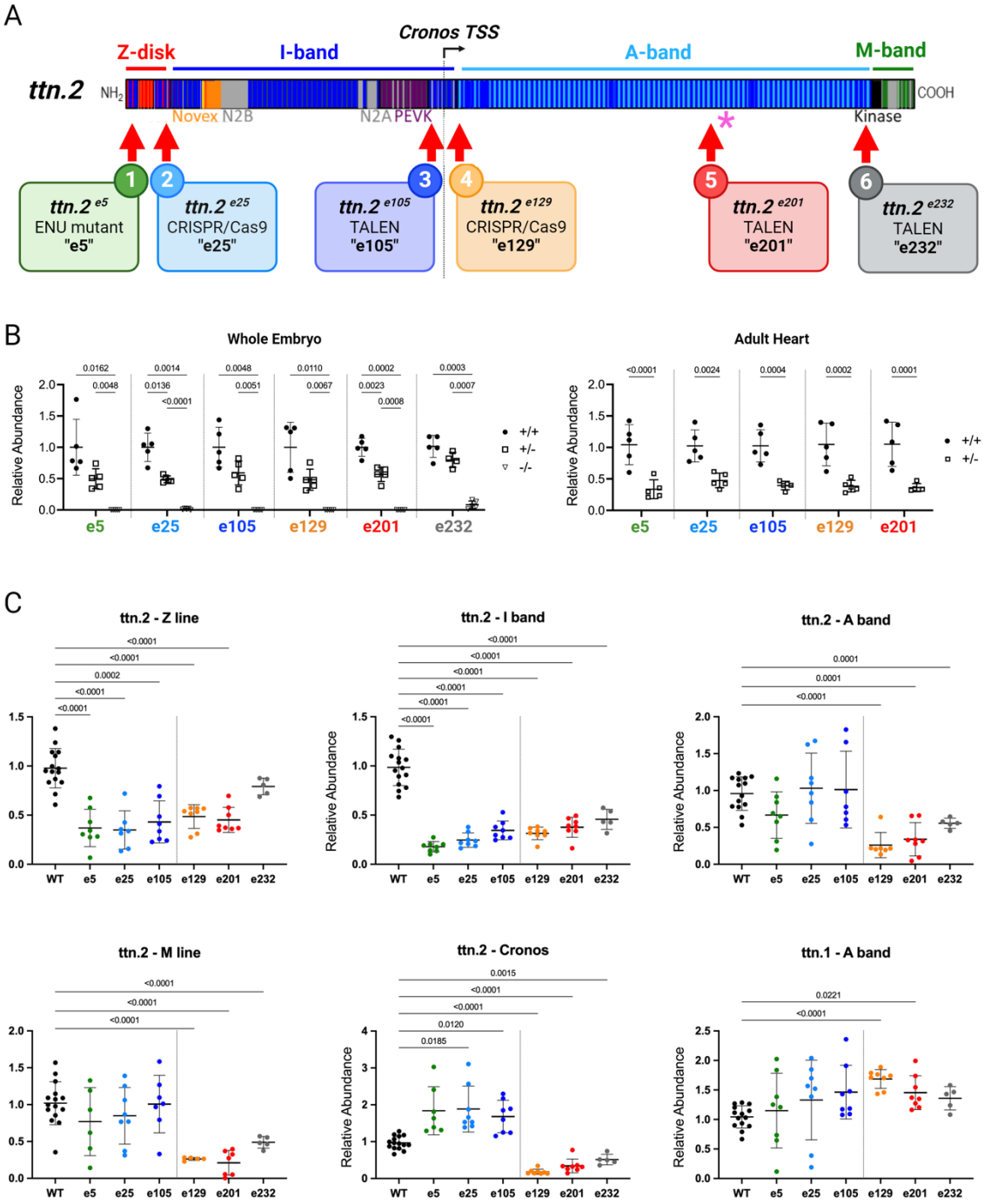
A
Cronos TSS
Z-disk
I-band
A-band
M-band
ttn.2
NH2
COOH
Novex N2B
N2A PEVK
Kinase
ttn.2 e5
ENU mutant
"e5"
ttn.2 e25
CRISPR/Cas9
"e25"
ttn.2 e105
TALEN
"e105"
ttn.2 e129
CRISPR/Cas9
"e129"
ttn.2 e201
TALEN
"e201"
ttn.2 e232
TALEN
"e232"
B
Whole Embryo
Adult Heart
Relative Abundance
+/+
+/-
-/-
e5
e25
e105
e129
e201
e232
C
ttn.2 - Z line
ttn.2 - I band
ttn.2 - A band
ttn.2 - M line
ttn.2 - Cronos
ttn.1 - A band
WT

Figure 2

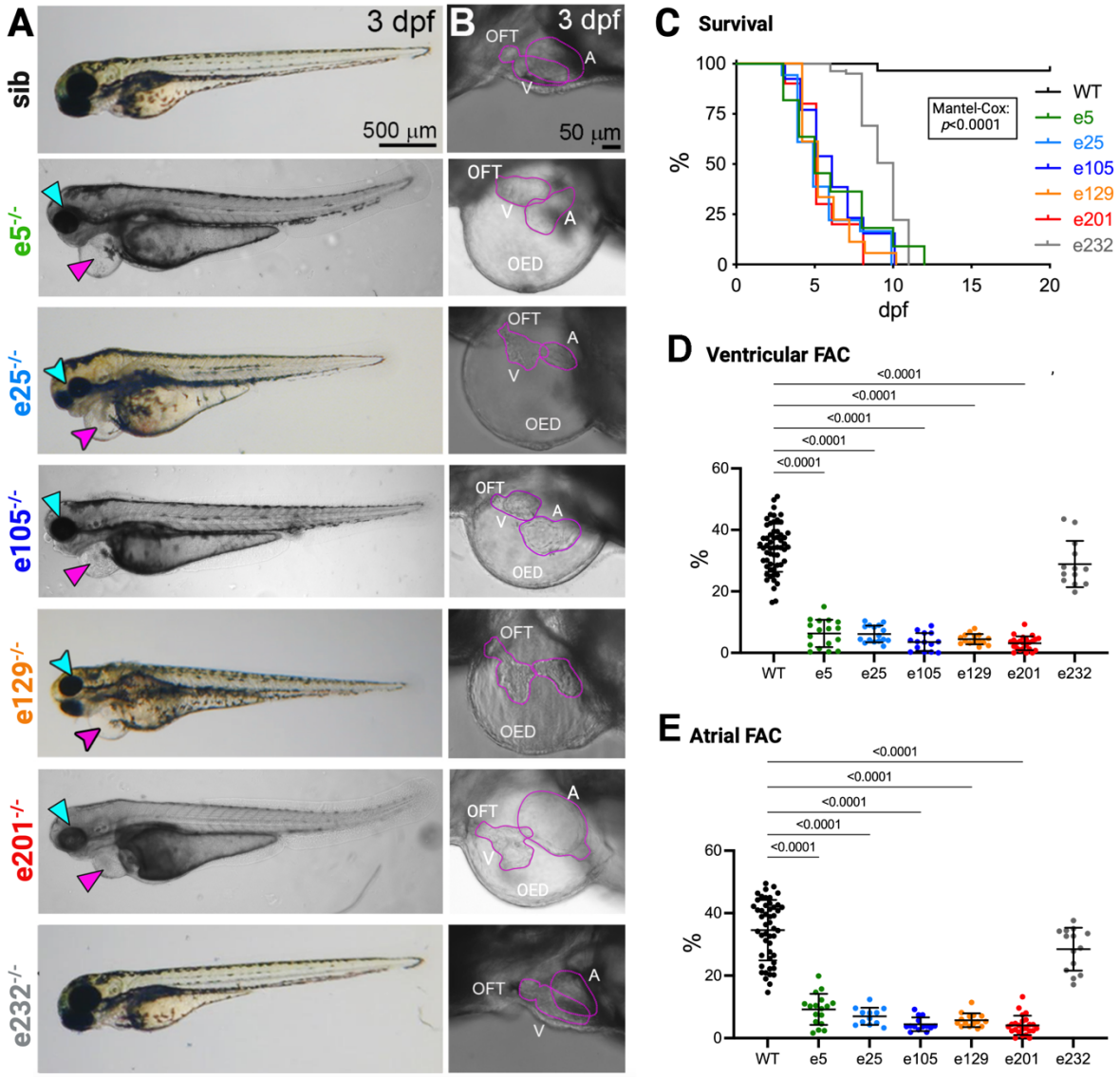
A
3 dpf
500 µm
B
3 dpf
50 µm
sib
e5-/-
e25-/-
e105-/-
e129-/-
e201-/-
e232-/-
OFT
A
V
OED
C Survival
Mantel-Cox: p<0.0001
WT
e5
e25
e105
e129
e201
e232
%
dpf
D Ventricular FAC
<0.0001
E Atrial FAC

Figure 3

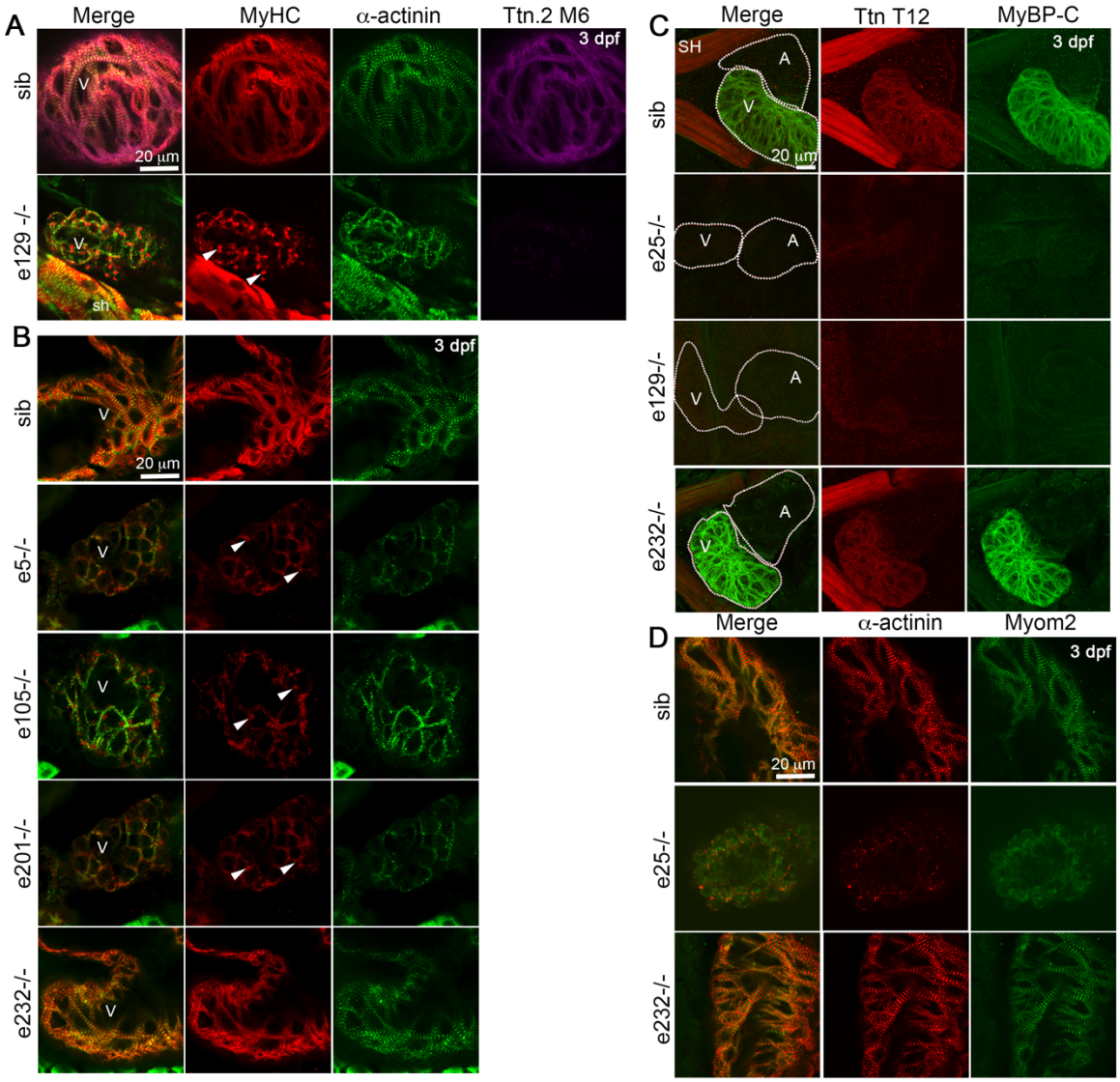
A
Merge
MyHC
α-actinin
Ttn.2 M6
3 dpf
sib
e129 -/-
V
sh
20 µm
B
3 dpf
sib
e5-/-
e105-/-
e201-/-
e232-/-
C
Merge
Ttn T12
MyBP-C
SH
A
V
e25-/-
e129-/-
e232-/-
D
Merge
α-actinin
Myom2

Figure 4

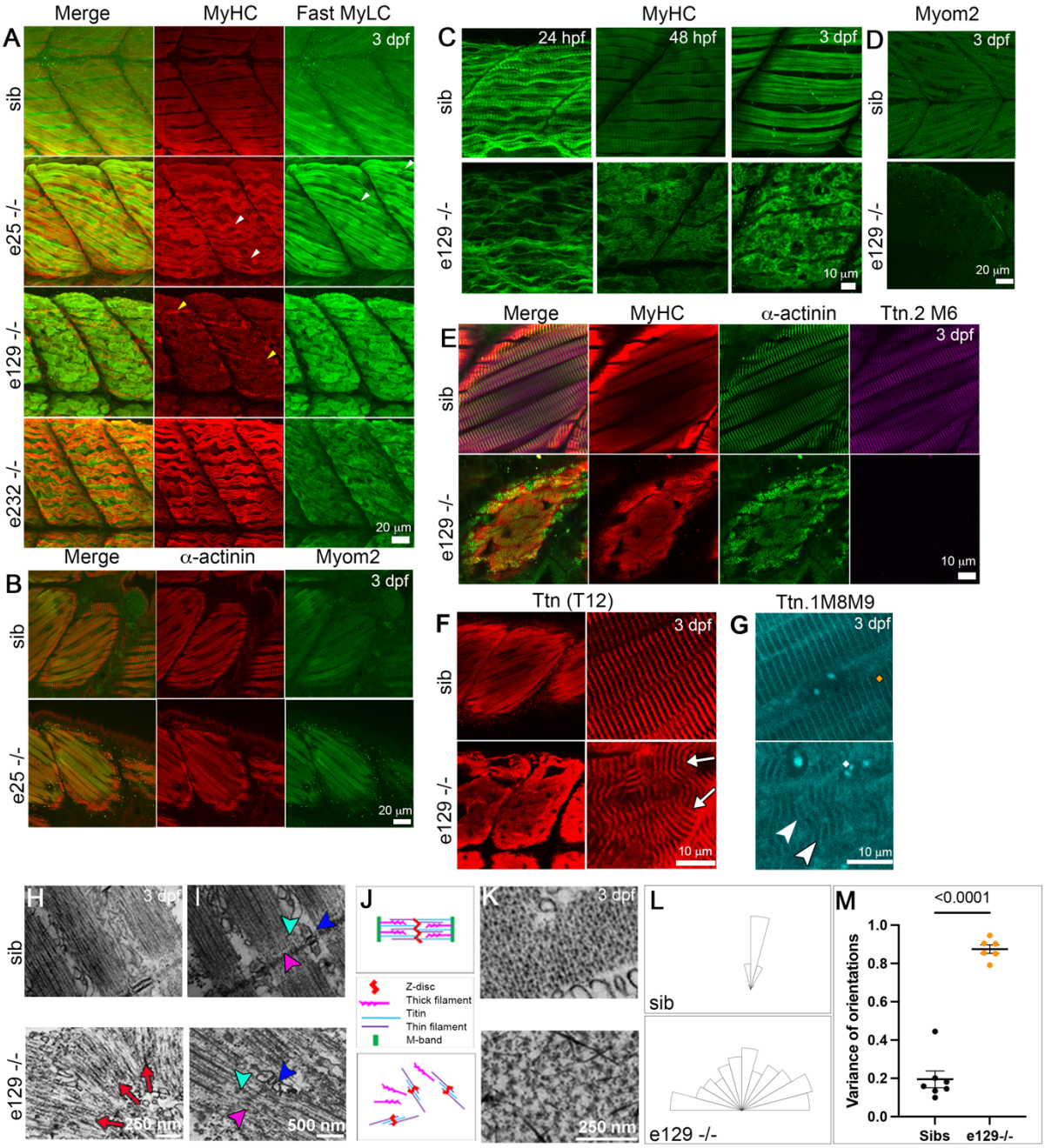
A
Merge
MyHC
Fast MyLC
3 dpf
sib
e25 -/-
e129 -/-
e232 -/-
20 µm
B
Merge
α-actinin
Myom2
3 dpf
sib
e25 -/-
20 µm
C
MyHC
24 hpf
48 hpf
3 dpf
sib
e129 -/-
10 µm
D
Myom2
3 dpf
sib
e129 -/-
20 µm
E
Merge
MyHC
α-actinin
Ttn.2 M6
3 dpf
sib
e129 -/-
10 µm
F
Ttn (T12)
3 dpf
sib
e129 -/-
10 µm
G
Ttn.1M8M9
3 dpf
10 µm
H
3 dpf
sib
e129 -/-
250 nm
I
500 nm
J
Z-disc
Thick filament
Titin
Thin filament
M-band
K
3 dpf
250 nm
L
sib
e129 -/-
M
<0.0001
Variance of orientations
1.0
0.8
0.6
0.4
0.2
0.0
Sibs
e129-/-

Figure 5

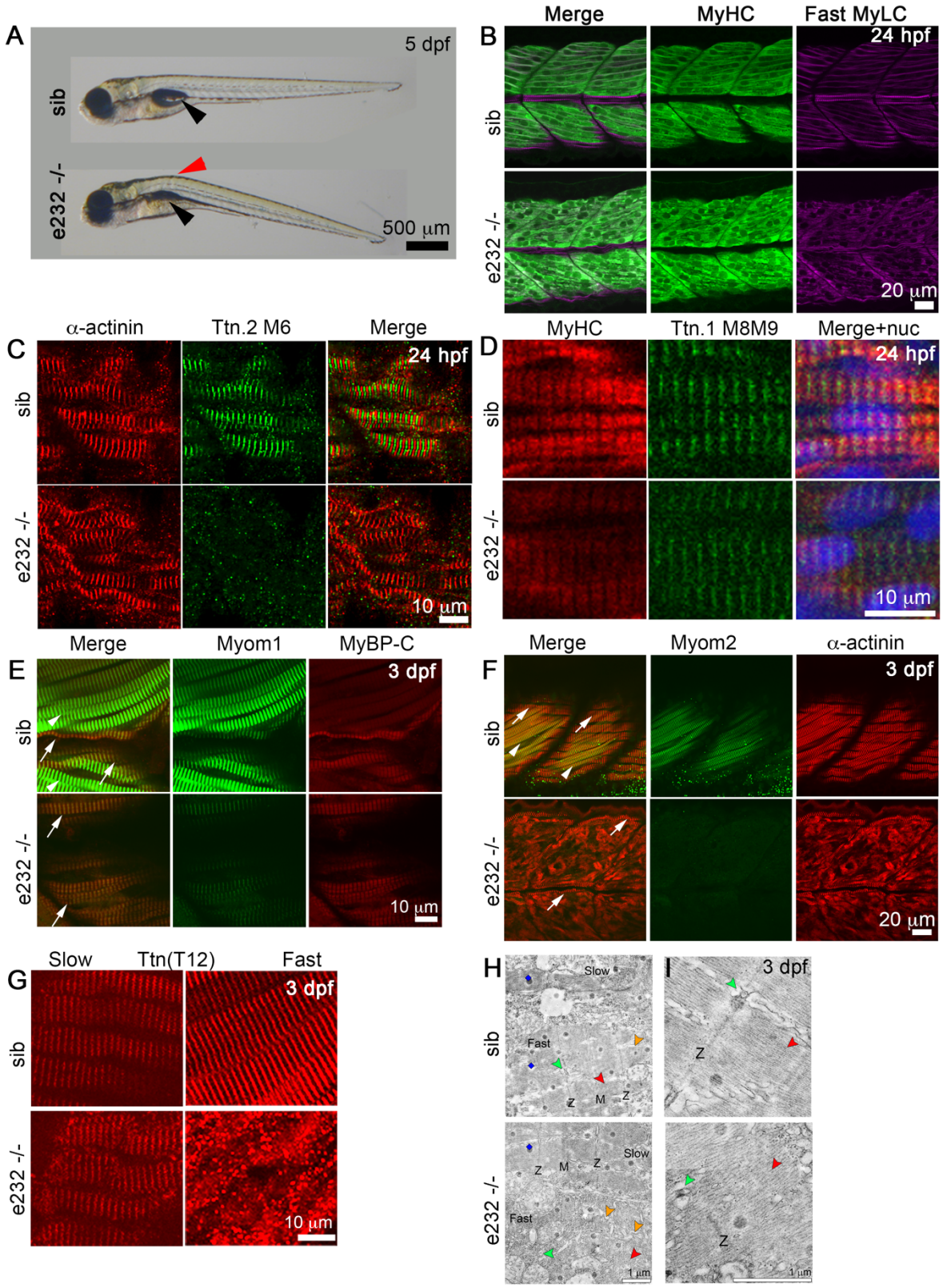
A
5 dpf
sib
e232 -/-
500 µm
B
Merge
MyHC
Fast MyLC
24 hpf
sib
e232 -/-
20 µm
C
α-actinin
Ttn.2 M6
Merge
24 hpf
sib
e232 -/-
10 µm
D
MyHC
Ttn.1 M8M9
Merge+nuc
24 hpf
sib
e232 -/-
10 µm
E
Merge
Myom1
MyBP-C
3 dpf
sib
e232 -/-
10 µm
F
Merge
Myom2
α-actinin
3 dpf
sib
e232 -/-
20 µm
G
Slow
Ttn(T12)
Fast
3 dpf
sib
e232 -/-
10 µm
H
Slow
Fast
Z
M
Z
sib
e232 -/-
1 µm
I
3 dpf
Z
Z
1 µm

Figure 6

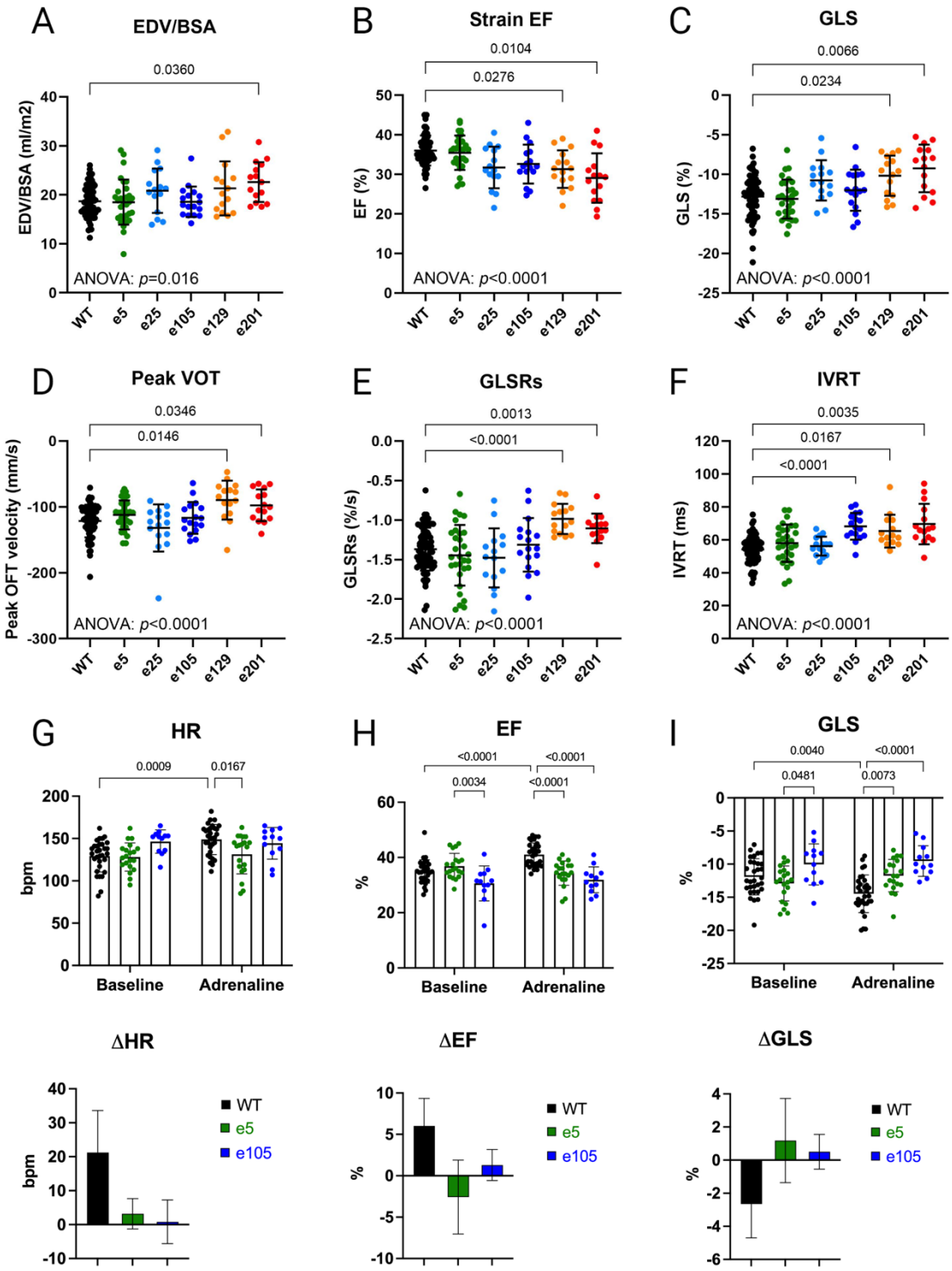
A
EDV/BSA
0.0360
EDV/BSA (ml/m2)
ANOVA: p=0.016
WT e5 e25 e105 e129 e201
B
Strain EF
0.0104
0.0276
EF (%)
ANOVA: p<0.0001
C
GLS
0.0066
0.0234
GLS (%)
ANOVA: p<0.0001
D
Peak VOT
0.0346
0.0146
Peak OFT velocity (mm/s)
ANOVA: p<0.0001
E
GLSRs
0.0013
<0.0001
GLSRs (%/s)
ANOVA: p<0.0001
F
IVRT
0.0035
0.0167
<0.0001
IVRT (ms)
ANOVA: p<0.0001
G
HR
0.0009
0.0167
bpm
Baseline
Adrenaline
H
EF
<0.0001
<0.0001
0.0034
<0.0001
%
Baseline
Adrenaline
I
GLS
0.0040
<0.0001
0.0481
0.0073
%
Baseline
Adrenaline
ΔHR
bpm
WT
e5
e105
ΔEF
%
WT
e5
e105
ΔGLS
%
WT
e5
e105